Precision Measurement of (Net-)proton Number Fluctuations in Au+Au Collisions from BES-II Program at RHIC-STAR

Bappaditya Mondal* for the STAR Collaboration[1,2]

[1]School of Physical Sciences, National Institute of Science Education and Research, Jatni 752050, India
[2]Homi Bhabha National Institute, Training School Complex, Anushaktinagar, Mumbai 400094, India

Abstract

We report precision measurements of cumulants (C_n) and factorial cumulants (κ_n) of (net-)proton multiplicity distribution upto fourth order in Au+Au collisions with $\sqrt{s_{NN}}$ =7.7 - 27 GeV measured by the STAR experiment from second phase of Beam Energy Scan program (BES-II) at RHIC. Using the high statistics data collected with upgraded detectors, we select protons and antiprotons at mid-rapidity $|y| < 0.5$ within $0.4 < p_T(GeV/\text{c}) < 2.0$. The dependence of measured cumulants and factorial cumulants on the collision energy are presented. The measured data are compared with calculations from lattice QCD, and expectations from various non-critical point models, such as the transport model UrQMD and the thermal model HRG.

1 Introduction

The Quantum Chromodynamics (QCD) phase diagram features at least two phases: the hadronic phase, where quarks and gluons are confined inside hadrons, and the quark-gluon plasma (QGP), where they exist in a deconfined state [1]. Lattice QCD calculations indicate that the transition between these two phases is a smooth crossover at small baryon chemical potential ($\mu_B \sim 0$) [2]. At higher μ_B, theoretical models based on QCD predict a first-order phase transition that ends at a critical point [3, 4]. Investigating this phase structure is a major objective in heavy-ion collision research. To explore such transitions, event-by-event fluctuations in the number of conserved charges are studied using higher-order cumulants (C_n), which are known to be sensitive to critical phenomena [5, 6]. Constructing ratios of these cumulants helps remove the influence of system volume and allows for direct comparison with susceptibility ratios (χ_n) calculated from lattice QCD and other theoretical models [7, 8]. Model-based study suggests that a non-monotonic variation on collision energy of fourth- to second-order net-proton cumulant ratio (C_4/C_2) with respect to baseline expectations could happen near the QCD critical point [9]. In the first phase of the Beam Energy Scan (BES-I) program at RHIC, the STAR experiment observed a hint of non-monotonic energy dependence in the net-proton C_4/C_2 ratio [10]. However, due to large uncertainties at lower collision energies, high-precision measurements are necessary to draw firm conclusions.

This proceedings article presents precise measurements of cumulants up to the fourth order ($C_n, n <= 4$) from net-proton multiplicity distributions in Au+Au collisions within the center-of-mass energy range $\sqrt{s_{NN}}$ = 7.7 to 27 GeV [11]. The data are collected by the STAR experiment operating in collider mode during the second phase of the Beam Energy Scan program

*bappaditya.mondal@niser.ac.in

(BES-II) at RHIC. These measurements benefited from key detector upgrades, most notably the upgradation of the inner sectors of the Time Projection Chamber (iTPC). In addition to regular cumulants, we also report proton factorial cumulants. These are expressed as $\kappa_1 = C_1$, $\kappa_2 = -C_1 + C_2$, $\kappa_3 = 2C_1 - 3C_2 + C_3$, and $\kappa_4 = -6C_1 + 11C_2 - 6C_3 + C_4$. Factorial cumulants of order n represent true n-particle correlations, whereas regular cumulants of the same order also include contributions from lower-order correlations.

2 Analysis Details

The primary vertex along beam direction (denoted as V_z), is required to be within ± 50 cm from the center of the STAR detector for all energies, except at $\sqrt{s_{NN}} = 27$ GeV, where a tighter range of ± 27 cm is applied to maintain uniform acceptance and efficiency of the Time Projection Chamber (TPC). A total of 45, 78, 116, 178, 116, 270, and 220 million minimum-bias events are analyzed for $\sqrt{s_{NN}} = 7.7$, 9.2, 11.5, 14.6, 17.3, 19.6 and 27 GeV, respectively—accounting for a 7 to 18 times increase in statistics compared to those in BES-I. Protons and antiprotons are selected at mid-rapidity ($|y| < 0.5$) within the transverse momentum range $0.4 < p_T < 2.0$ GeV/c. For low-p_T particles ($0.4 < p_T < 0.8$ GeV/c), particle identification was performed using ionization energy loss (dE/dx) in the TPC. For higher-p_T particles, both TPC and Time-of-Flight (TOF) detectors are used. This combined method ensures a particle purity of approximately 99% across the full kinematic acceptance.

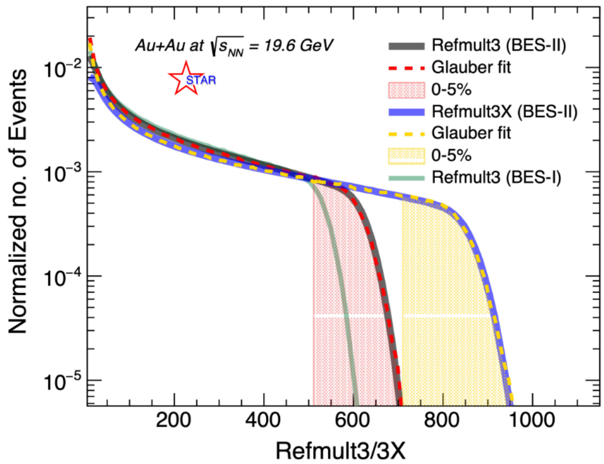

Figure 1: The distribution of charged particle multiplicity. The shaded region represents the 0–5% most central collision events. Glauber model fits are also shown.

Figure 1 presents the charged particle multiplicity distributions, labeled as RefMult3 and RefMult3X. These distributions are based on the number of charged particles detected within $|\eta| < 1.0$ for RefMult3 and $|\eta| < 1.6$ for RefMult3X, excluding protons and antiprotons to avoid self-correlation effects. Since higher multiplicity improves the resolution of centrality determination, RefMult3X provides a better centrality resolution. Centrality classes are determined by comparing the measured multiplicity distributions with those generated from Glauber model simulations [12]. To account for variations within wide centrality bins, a centrality-bin-width correction (CBWC) was applied on measurements with a given centrality class [13]. The measured cumulants are corrected for the finite efficiency of the detector by assuming a binomial detector response [14]. Statistical uncertainties are estimated using the bootstrap method. Systematic uncertainties are evaluated by varying criteria for track reconstruction, particle identification (PID) and reconstruction efficiencies.

3 Results

The left panel of Figure 2 illustrates the variation of the net-proton C_4/C_2 ratio as a function of collision energy for both central (0–5%) and peripheral (70–80%) Au+Au collisions. Measurements from $\sqrt{s_{NN}} = 7.7$ to 27 GeV are taken during BES-II, while those at higher energies are from BES-I. For BES-II, RefMult3X is used for centrality determination, with the exception of $\sqrt{s_{NN}} = 27$ GeV, where RefMult3 is utilized due to the unavailability of the iTPC detector upgrade. The results exhibit a pronounced deviation from the Poisson expectation at unity. In central collisions, the C_4/C_2 ratio tends to decrease as the energy is lowered, although a modest increase is hinted at lower energies, with considerable uncertainties. The data are compared with models that do not include a critical point—such as UrQMD [15], HRG with canonical ensemble (HRG CE) [16], and hydrodynamics with excluded volume (Hydro EV) [17]—all of which implement exact baryon number conservation. None of these models fully reproduce the energy dependence trend observed in the data.

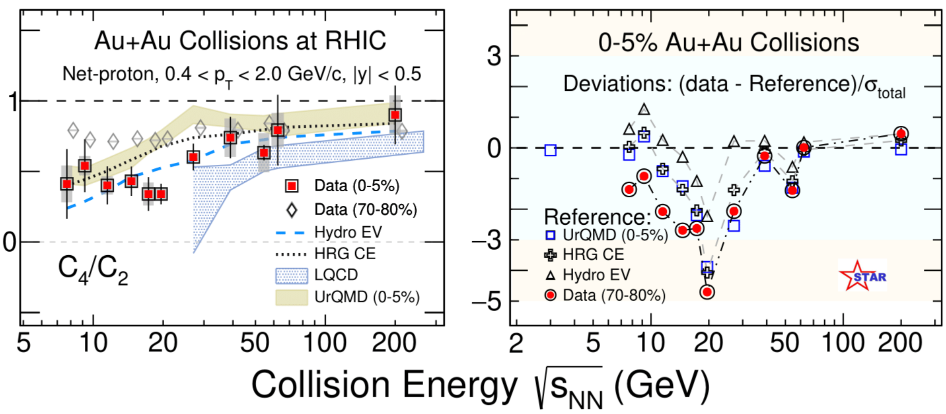

Figure 2: Left: Collision energy dependence of net-proton C_4/C_2. Also shown are Hydro EV results (blue dashed), HRG CE calculations (black dotted), UrQMD predictions (brown band), and lattice QCD estimates (light-blue band). Right: Significance of deviation (data − reference)/σ_{total} for net-proton C_4/C_2. Reference include UrQMD (blue squares), HRG CE (black crosses), Hydro EV (black triangles), and 70–80% peripheral collision measurements (red dots).

The new results show a noticeable deviation from all these non-critical model expectations near $\sqrt{s_{NN}} \approx 20$ GeV. The deviation of net-proton C_4/C_2 from various non-critical baselines is shown in the right panel of Figure 2, where it is calculated as the difference between the 0–5% central collision data and the baseline values, normalized by the total uncertainty (σ_{total}). The baselines include predictions from UrQMD, HRG CE, and Hydro EV, as well as measurements from 70–80% peripheral collisions. The largest deviations, in the range of 2–5σ, are observed at $\sqrt{s_{NN}} = 19.6$ GeV across all references.

As stated above, factorial cumulants are also sensitive observables for critical point search. Figure 3 shows the energy dependence of the proton factorial cumulant ratios κ_2/κ_1, κ_3/κ_1, and κ_4/κ_1 for central (0–5%) and peripheral (70–80%) collisions. In the most central events, both κ_2/κ_1 and κ_3/κ_1 deviate significantly from the Poisson baseline at zero, while κ_4/κ_1 remains consistent with zero across all energies within uncertainties. The peripheral measurements are closer to zero. UrQMD calculations do not fully capture these observed trends.

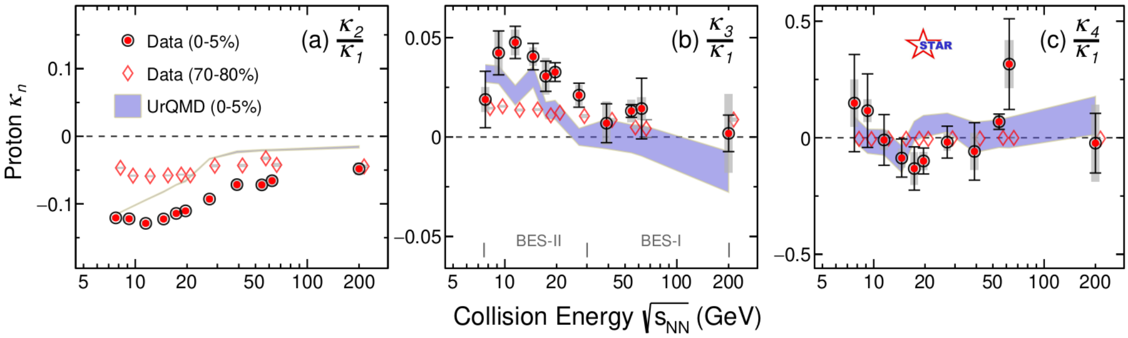

Figure 3: Collision energy dependence of proton factorial cumulant ratios κ_2/κ_1, κ_3/κ_1, and κ_4/κ_1. UrQMD predictions are shown in band.

4 Summary

In summary, we presented high-precision measurements of net-proton cumulants and proton factorial cumulants from BES-II over the center-of-mass energy range of $\sqrt{s_{NN}} = 7.7$–27 GeV, corresponding to baryon chemical potentials (μ_B) of approximately 400–150 MeV. The analysis benefits from improved statistical precision, enhanced centrality resolution, and better control of systematic uncertainties. The deviation of net-proton C_4/C_2 $(0-5\%)$ from non-critical models and peripheral data (70–80% centrality) is observed at $\sqrt{s_{NN}} = 19.6$ GeV ($\mu_B \approx 206$ MeV), reaching a significance of 2–5σ. Proton factorial cumulant ratios show deviations from the Poisson baseline and their energy dependence cannot be fully explained by UrQMD. To interpret these observations, dynamical model calculations incorporating critical point are essential. Additionally, measurements of higher moments at further lower energies (high baryon density) are crucial in the search for the QCD critical point.

References

[1] A. Pandav, D. Mallick, and B. Mohanty. *PPNP* 125 (July 2022), p. 103960.

[2] Y. Aoki et al. *Nature* 443.7112 (Oct. 2006), pp. 675–678.

[3] Shinji Ejiri. *PRD* 78 (7 Oct. 2008), p. 074507.

[4] E. S. Bowman and J. I. Kapusta. *PRC* 79 (1 Jan. 2009), p. 015202.

[5] M. A. Stephanov. *PRL* 107 (5 July 2011), p. 052301.

[6] A. Bazavov et al. *PRD* 101 (7 Apr. 2020), p. 074502.

[7] S. Gupta et al. *Science* 332.6037 (June 2011), pp. 1525–1528.

[8] F. Karsch and K. Redlich. *PLB* 695.1–4 (Jan. 2011), pp. 136–142.

[9] M. A. Stephanov. *PRL* 107.5 (July 2011).

[10] J. Adam et al. *PRL* 126 (9 Mar. 2021), p. 092301.

[11] STAR Collaboration (2025). arXiv:2504.00817.

[12] Michael L. Miller et al. *Ann. Rev. NPS.* 57.1 (Nov. 2007), pp. 205–243.

[13] Xiaofeng Luo et al. *JPG* 40 (2013), p. 105104.

[14] T. Nonaka, M. Kitazawa, and S. Esumi. *PRC* 95 (6 June 2017), p. 064912.

[15] S Bass. *PPNP* 41 (1998), pp. 255–369.

[16] P. Braun-Munzinger et al. *NPA* 1008 (Apr. 2021), p. 122141.

[17] V. Vovchenko, V. Koch, and C. Shen. *PRC* 105.1 (Jan. 2022).